RSC Advances

ROYAL SOCIETY OF CHEMISTRY

www.rsc.org/advances

Cite this: DOI: 10.1039/c0xx00000x

www.rsc.org/xxxxxx

ARTICLE TYPE

Self-Assembled Supramolecular Nanoparticles Mediated by Host–Guest Interactions for Photodynamic Therapy

Hong Yan, [a] Xiaoyong Pan, [a] Ming Hui Chua, [a] Xiaobai Wang, [a] Jing Song, [a] Qun Ye, [a] Hui Zhou, [a] Angeline TAN Yan Xuan, [a] Ye Liu [a] and Jianwei Xu*[a,b]

Received (in XXX, XXX) Xth XXXXXXXXX 20XX, Accepted Xth XXXXXXXXX 20XX
DOI: 10.1039/b000000x

This paper describes a facile and reproducible protocol for the preparation of supramolecular photodynamic therapeutic agent mediated by host-guest encapsulation in the absence of inorganic matrix. Two distinct approaches were explored to modulate the size and morphology of supramolecular nanoparticles (SNPs). One approach is through changing the guest integration components of biviologen derivatives during the self-assembly process. It provides the opportunity to modulate the morphology (from amorphous to spherical) and the size of self-assemblies (from 100 to 600 nm) by simply adjusting the length of guest components. The other approach is a facile oil-in-water emulsion-phase method to synthesize high-quality supramolecular photodynamic therapeutic agents with good dispersion and uniform morphology in aqueous solution. In particular, photosensitizing efficiency was compared and the results revealed that this kind of particles exhibited higher photo-oxidation efficiency than its pure porphyrin derivative at the same concentration. Furthermore, the confocal microscopic images revealed the SNPs can be successfully endocytosed by Hela cell at various concentrations. In addiation, the MTT assay indicated cell viability was not hindered by the concentration of SNPs up to 3.2 mg/mL before light irradiation, thereby revealing good biocompatibility and remarkably low cytotoxicity of SNPs in vitro. Importantly, the cell viability was significantly attenuated to ~20% after light irradiation (633 nm) for 1 hour. This type of SNPs would thus be promising materials as supramolecular photodynamic therapeutic agents in the treatment of cancer.

1. Introduction

Photodynamic therapy (PDT) currently represents an alternative or complementary therapeutic approach in the treatment of cancer in clinical trials, mainly owing to their promising features which are minimally invasive and minimally toxic.[1] At present, most modern PDT applications basically consist of three key components: i) nontoxic light-sensitive drugs (called a photosensitizer or photosensitizing agent), ii) a particular type of light, and iii) reactive oxygen species such as singlet oxygen or free radicals.[2a] The crucial point in PDT systems is that the photosensitizer can be easily excited to produce the reactive oxygen species under light irradiation at an appropriate wavelength, which can then oxidize cell compartment components and cause irreversible damage to tumour cells.[2b] To date, haematoporphyrin derivatives and their purified fractions (Photofrin) with absorbance in the red region of the spectrum have been widely employed as photosensitisers for applications in clinical PDT due to their good cytotoxic oxygen species generation and exhibition of no dark toxicity.[3,4] It is interestingly that once exposed in vivo in the presence of haematoporphyrin derivatives, a number of the latter therapeutics exhibited increased selectivity for malignant tissue over normal tissue.

Despite these advantages, however, the application of the photosensitizer delivery systems in clinical PDT still suffers from several drawbacks. The current major challenge of engineering photosensitizer delivery systems in PDT processes is how to avoid the aggregation propensity of most hydrophobic photosensitizers in the physiological environment, which may lead to inhomogeneous distribution of photosensitizer in tumour cells as well as significant reduction of photo-sensitization efficiency.[5, 6] Furthermore, some photosensitizers have potential toxicity to healthy tissues and shorten retention in the tumour. Typically due to the low permeability and short residence time of most organic dyes in vitro and in vivo, developing a new strategy to improve the therapeutic efficiency of the photosensitizers is strongly needed.

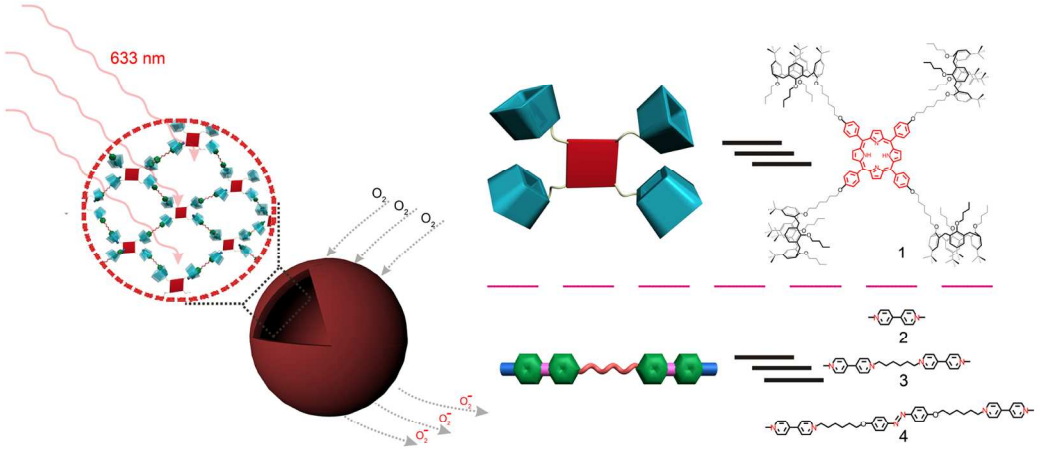

Figure 1. A graphical representation of generation of spheral supramolecular nanoparticles through host-guest interactions between calix[4]arene-decorating containing tetrameric porphyrin derivative 1 and different length of biviologen derivatives **2** ~ **4**.

To overcome these limitations, recent work has been focused on loading or capping the photosensitizers in certain nanocarriers, notable examples including mesoporous silica nanoparticles,[7] liposomes[8] and polymeric micelles[9, 10], etc. To a certain extent, the nanocarriers can enhance uptake of photosensitizer by tumour cells and increase cytotoxicity to tumour tissues as compared to pure photosensitizer dispersion.[11] Nevertheless, photosensitizers encapsulated in nanocarriers may self-aggregate and thus lead to significant reduction of photosensitizing efficiency. Therefore, it is desirable to develop new types of carriers in which the photo sensitizers can be homogeneously dispersed and self-aggregate can be suppressed so that the photosensitizing efficiency can be maintained.

In recent years, improvements in degradability, stimuli-responsiveness, and self-healing of supramolecular organic frameworks favored manipulation of the noncovalent forces that hold the monomeric units together.[12, 13] Calixarene-based molecular architectures have been widely studied for both molecular and ionic recognition since their π-rich cavities.[14] However, to the best of our knowledge, construction of haematoporphyrin hybrid supramolecular complexes with controllable morphology as PDT therapeutic agents has not been explored. Thus, there is a considerable interest in incorporating photosensitizing haematoporphyrin fraction into supramolecular complexes, and exploring their potential application in clinical PDT.[15] However, the construction of supramolecular nanoparticles by using haematoporphyrin tailored calix[4]arene as host molecules and corresponding cationic guest molecules through host-guest recognition with controllable morphology and biological permeability still poses a considerable challenge to chemists. Moreover, the development of haematoporphyrin-based supramolecular systems that exhibit low toxicity and high photosensitizing efficiency by convenient strategy is of the highest importance.

2. Experimental Section

General Methods and Materials.

All chemicals were purchased commercially and used as received unless otherwise mentioned. All reactions for the synthesis of different functional molecules were carried out under an atmosphere of nitrogen unless otherwise specified. The ^{1}H NMR and ROESY NMR spectra were recorded on a Bruker 400 MHz NMR at room temperature and chemical shifts were recorded in parts per million (ppm). Mass spectra were recorded using ESI mode carried out on a ThermoFinnigan LCQ quadrupole ion trap mass spectrometer. UV-vis absorption analyses were performed on a Shimadzu UV-3600 UV-Vis-NIR spectrophotometer (1 cm quartz cell used). Fluorescence spectra were recorded on a Perkin-Elmer Instrument LS 55 luminescence spectrometer. The Olympus Fluoview FV300 confocal microscope was used to image the polymer-labeled Hela cells. Scanning electron microscopic (SEM) images of SNPs were captured on a LEO 1530 field emission scanning electron microscope (FESEM) (LEO Elektronenmikroskopie GmbH, Oberkochen, Germany) at an accelerating voltage of 5 kV.

Synthetic procedure of intermediates and calix[4]arene derivatives

In the present work, 25-[(6-bromohexyl)oxy]-26,27,28-tributyloxy-*p*-*tert*-butyl-calix[4]arene **5** was used in cooperation with 5,10,15,20-tetrakis(4-hydroxyphenyl)porphyrin **7** to yield a novel calix[4]arene-substituted tetrameric porphyrin structures **1**. The *mono*-*6*-bromohexyl substituted *p*-*tert*-butyl-calix[4]arene **5** was prepared according to the synthetic route shown in Scheme 1. Firstly, tributane-substituted *p*-*tert*-butyl-calix[4]arene **6** was synthesized and purified according to the literature procedures.[16] Then, **6** reacted with **4** equivalents of 1,6-dibromohexane in the presence of NaH in dry DMF at 50 °C to afford 25-[(6-bromohexyl)oxy]-26,27,28-tributyloxy-*p*-*tert*-butyl-calix[4]arenes **5** in good yield (88 %). This compound was subsequently used as the starting materials in reaction with 5,10,15,20-tetrakis(4-hydroxyphenyl)porphyrin in the presence of K_2CO_3 in dry DMF at 100 °C for the preparation of the corresponding *tetra*-calix[4]arene-substituted porphyrin **1** (13 %) (Scheme 1). Biviologen derivatives **2** ~ **4** with different length for the control study were synthesized according to the literature reported method.[17] The intermediates and target compound were fully characterized by NMR spectroscopy and ESI-Mass spectrometry.

Nanoparticle formation

Two methods were utilized to study the influences of guest components on the morphology of SNPs. (1) Drop coating method. Different concentration of Me_2CO solution containing the complex of tetra-calix[4]arene-substituted porphyrin **1** and a variety of biviologen derivatives was dropped onto a glass slide, and then allowed to air-dry. The process of self-assembly spontaneously creates well-defined morphology from various host-guest building blocks. In this way particle formation is rapid, highly tunable and does not require protection chemistries. (2) Oil-in-water emulsion-phase method. Briefly, the above 0.5 mL solution of complextion of host-gust was then emulsified with 2 mL of water. The cationic biviologen derivatives with different lengths serve as structure-directing agents for oligomerization by electrostatic interaction. Particle morphology was monitored by fluorescence microscopy, transmission electron microscopy (TEM) and scanning electron microscopy (SEM).

Cell viability assay

Hela cells were used in this investigation and they were cultured in DMEM media at 37 ^{o}C in 5 % CO_2 humidified atmosphere. The cytotoxicity of SNPs was then assessed through MTT assay. Different concentrations of SNPs in Dulbecco's Modified Eagle Medium (DMEM) were prepared via serial dilution. 7 concentrations ranging from 0.05 mg/mL to 3.2 mg/mL were used for cell viability assay. Initially, Hela cells were seeded in a 96-well plate with 100 μL DMEM as the media, at a density of 1×10^4 cells/well and incubated for 24 hours. The culture medium DMEM in each well was then replaced by 100 μL of SNPs solution in DMEM at prescribed concentration. After incubation for 3 days, 10 μL of MTT solution was added into each well followed by incubation for 4 hours. All of the solution in each well was then removed and replaced with 100 μL of DMSO. Finally, the 96-well plate was then placed onto plate shaker (1000 rpm, 5 mins). The absorbance of each well was measured at 490 nm using a Synergy HT Multi-Mode Microplate Reader (BioTek, USA). Non-treated cell in DMEM and pure DMEM was used as a control and blank with 100% and 0% cell viabilities respectively. The relative cell viability was expressed as (Abs sample-Abs blank)/(Abs control-Abs blank).

3. Results and Discussion

Recently, chemists found that the host and guest derivatives might be utilized as useful building blocks for the design and synthesis of novel supramolecular morphology with specific structures and properties.[18] Host-guest interaction between the cavities and corresponding guests is the main driving force during the course of self-assembly.[19] Especially, multi-host moiety structure is particularly interesting due to their expansionary properties in contrast to the linear molecules with the same molecular weight. For example, Zhang et al conducted host–guest complexation between pillararene trimer and biviologen derivatives to fabricate the dynamic supramolecular self-assembly, which exhibits a reversible multidimensional transformation from 0 D to 3 D upon concentration changes.[20] In this regard, enormous efforts have been made to construct highly complex nano-supramolecular assemblies with calix[n]arene based hosts and certain gusets by Liu's group.[21, 22] Nevertheless, the amorphous or non-uniform morphology of complexation limits its practical biomedical applications.

In the light of such fascinating examples and their potential applications of complexation in PDT, we herein employed three-dimensional calix[4]arene as a building host block because its π-rich cavities can strongly bind to organic cations. Furthermore, calix[4]arene and its derivatives with preferred stable cone conformation have been widely used to construct supramolecular nanoarchitectures with well-defined geometries.[23] As a result of the incorporation of terminated calix[4]arene moiety as a recognition-anchoring group and porphyrin fraction served as the central unit, compound **1** has proved to be powerful hosts for further promoting the formation of the cage-like host-guest paired complexes structure. As the inclusion complexes mainly originate from positive charges of biviologen devivertives, they are suitably matched to the π-rich cavity of calix[4]arenes. According literature report, the binding constant of calix[4]arene to viologen is around 280 ~ 320 M^{-1}.[24] In addition to functioning as photosensitizer, the presence of porphyrin segment centered on molecular networks could act as an active site which may facilitate self-assembly of complexes, making it suitable for PDT applications.

Host-Guest interaction of calix[4]arene and biviologen derivatives

Detailed studies to characterize and prove the cation-π assisted supramolecular self-assembly among calix[4]arene moiety and biviologen derivatives were assessed by examining the chemical shift (^{1}H NMR) and cross-peaks (2D ROESY NMR) upon introducing various guest groups. Three different host–guest groups were studied for morphology control and crosslinking

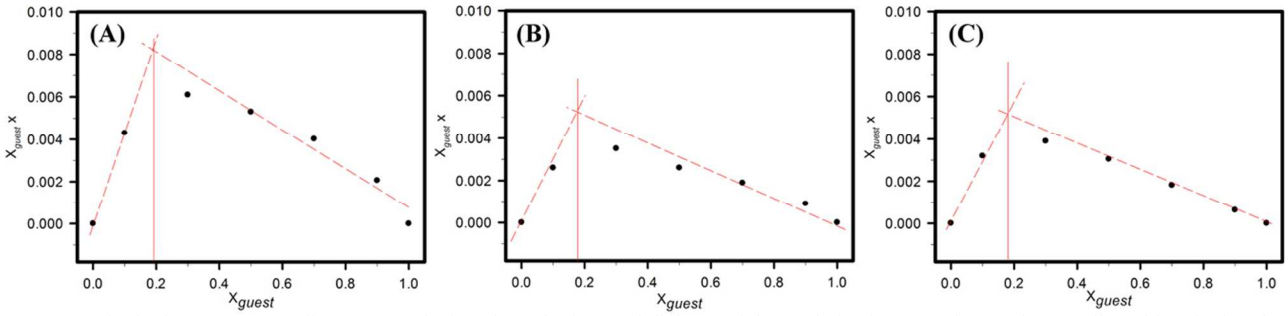

Figure 2. Job plot between tetra-calix[4]arene-substituted porphyrin **1** and different viologen derivatives a) **2**, b) **3** and c) **4** collected by plotting the Δδ in chemical shift of the viologen derivatives proton H_a, which was observed by ^{1}H NMR spectroscopy (Acetone-d_6) against the change in the mole fraction of the guest (X_{guest}). [Host] and [Guest] are concentrations of host molecule **1** and viologen derivatives **2**, **3** and **4**, respectively. The total concentration of host and guest molecules was kept at 20.0 mM in this titration ([Host]+[Guest]=20.0 mM).

reactivity, *i.e.* **1**–**2** group (G1), **1**–**3** group (G2), and **1**–**4** group (G3). To investigate the host-guest interactions, the complex of biviologen derivatives **2** with mono-calix[4]arene **5** was employed as the reference system (**2**–**5** group: G4). Me_2CO was chosen as the solvent for investigating the host–guest interactions due to the excellent solubility to biviologen derivatives.

In general, ^{1}H NMR titration of calix[4]arene into a solution of biviologen derivatives in acetone-D_6 provides an important insight into the nature of calix[4]arene, which exhibits excellent binding to the biviologen derivatives through cation-π interactions. The addition of the biviologen derivatives in a controlled concentration ratio into the solution of host component was found to produce a distinct change in the chemical shift evolution. For example, the ~ 0.1 ppm down shifts of the corresponding aromatic proton peaks H_{a-b} of the biviologen unit (**2**, **3** and **4**) in the presence of the calix[4]arene moieties (**1** and **5**) indicate the calix[4]arene ring partially encircles the biviologen dericatives in the solution. The ^{1}H NMR spectroscopic titrations further afforded a quantitative estimation of the complexation between host **1** and different guests by monitoring the changes of the chemical shift of the proton H_a of biviologen derivatives. It is particularly fascinating that the jobs plot indicates the tetra-calix[4]arene-substituted porphyrin **1** preferred 1 : 4 stoichiometries to form complex species with biviologen derivatives through programmable cation-π assisted molecular recognition. The above observation is in contrast to the case of **2**–**5** group (G4) in figure S1 where the jobs plot indicates 1 : 1 stoichiometries of the complexes formed between mono-calix[4]arene **5** and biviologen derivative **2**. Notably, the calix[4]arene moiety in **1** and **5** displays a cone-like configuration based on the characteristic ^{1}H NMR spectral pattern showing a pair of doublets (4.44 and 3.11 ppm) for the calix[4]arene bridging methylene protons, because of hydroxy groups locked by bulky substituents.[25]

Moreover, the 2D ROESY experiment of complex (20 mM total molar concentration, 1 : 4 molar ratio between host and guests) was carried out to further investigate the complexation between the host and guests. The cross-peaks between aromatic protons Ar-$H_{1,2}$ in the calix[4]arene ring of **1** and protons H_a and H_b in the biviologen derivatives of **2**, **3** and **4** can be observed in figure 3. Meanwhile, the weak cross-peaks between calix[4]arene bridging methylene protons $H_{3,4}$ of **1** and the protons H_a, H_b in biviologen units were also identified. This result suggests that a stable complex between *tetra*-calix[4]arene-substituted porphyrin **1** and biviologen derivatives existed in solution.

Preparation and Characterization of Supramolecular Nanoarchitectures

We documented that cation-π assisted molecular recognition can induce the oligomerization of *tetra*-calix[4]arene-substituted porphyrin **1** and biviologen derivatives with preferable 1 : 4 stoichiometries. This has significant potential in preparation of nanomaterials containing functional molecular entities that may be addressable or controllable. Herein we exploited well-

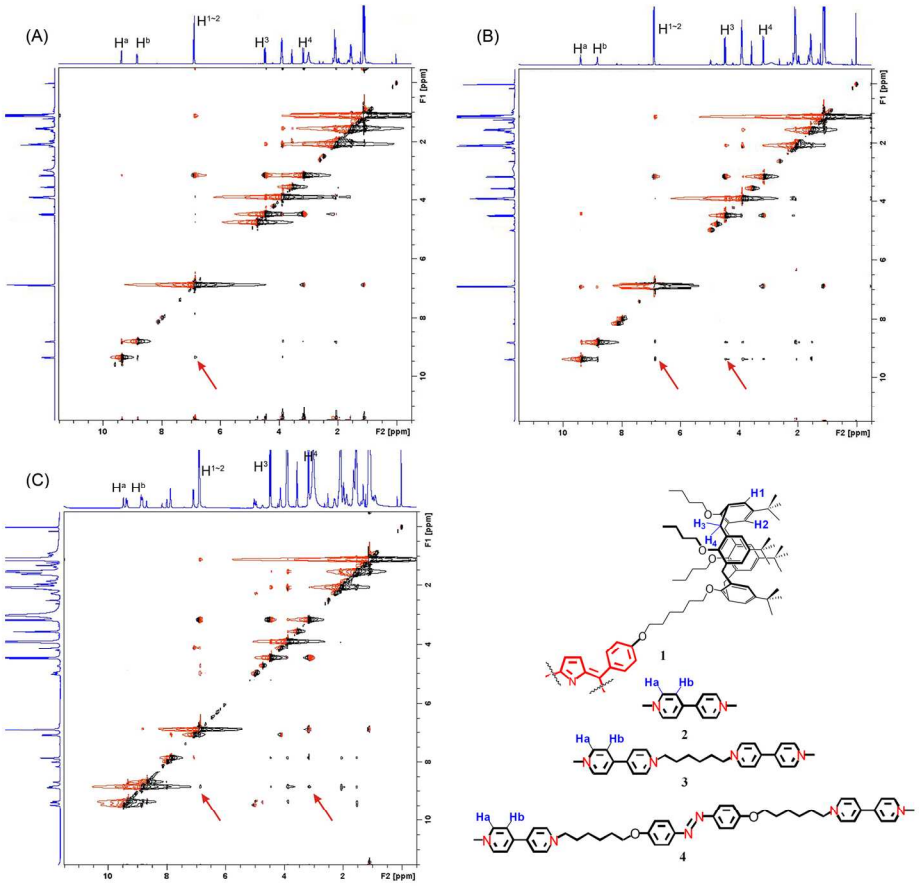

Figure 3. ROESY 2D NMR of biviologen derivatives (A) **2**, (B) **3** and (C) **4** with tetra-calix[4]arene-substituted porphyrin **1** (4:1 equiv.) in acetone-d_6 (400 MHz, 20 mM, 298 K).

established non-covalent interactions promoted self-assemblies, which have led to the formation of nanomaterials with controllable morphologies and novel properties. Furthermore, this approach enables the investigation of the structure-function relationship in the host-guests self-organized systems with minimal structural modification for the molecular components. In this study, two methods (drop coating and oil-in-water emulsion-phase method) were utilized to study the influences of guest components on the morphology of SNPs. The cationic biviologen derivatives with different lengths serve as structure-directing agents for oligomerization by electrostatic interaction. Interestingly, only diviologen derivative **4** (Group 3) was able to generate particles by the emulsion method. Under such conditions, the produced SNPs can be dispersed by homogenization in aqueous solution, which were illustrated in Figure S2.

Firstly, fluorescence microscopy was used to determine whether there were morphological differences between the tetra-calix[4]arene-substituted porphyrin **1** and various biviologen derivatives (G1 ~ G3) formed particulate states by monitoring the intense red fluorescence of **1** (figure S3). Figure 4 shows a representative set of the fluorescence microscopy images of self-assemblies synthesized by method I (figure A1~3) and method II (figure B1~3), respectively. Highly monodisperse and perfectly spherical fluorescent particulate entities were produced by method I, which was evident for these as-synthesized nanoparticles. Spherical structures with an average diameter of 204 ± 100 nm (G1), 207 ± 82 nm (G2) and 171 ± 100 nm (G3) were observed for biviologen derivatives **2**, **3** and **4** serving as structure-directing agents, respectively (Fig. A1~C1). Interestingly, the spherical morphologies did change obviously upon changing the concentrations of samples. In comparison with the particle size listed in Table 1, a statistical analysis of the size of the micelles at different concentrations showed an increased particle size with increasing concentrations of host-guest molecules. For the samples obtained with lower concentration 0.2 mM of host-guest complex at the same time, the SSNPs seem to be smaller and their shapes are irregular. Once the concentrations of host-guest complex were increased to 20 mM, a bimodal size distribution of nonuniform spherical SSNPs can be observed in Figure S4. In addition, the particles size did not show significant distinction among these three biviologen derivatives at the same concentration. This observation indicates that the length of the structure-directing agents in the self-assembly process would not be the key factor to determine the particle size.

Table 1. Summary of particle size observed by fluorescent microscopy [a]

Group	*0.2 mM*	*2 mM*	*20 mM* [b]
G1	151 ± 80 nm	204 ± 100 nm	189 ± 102 nm 364 ± 66 nm
G2	55 ± 102 nm	207 ± 82 nm	219 ± 103 nm 564 ± 18 nm
G3	205 ± 100 nm	171 ± 100 nm	251 ± 74 nm 1387 ± 28 nm

[a] SNPs were formed under different concentration prepared by method I; [b] Bimodal size distribution was observed at high concentration.

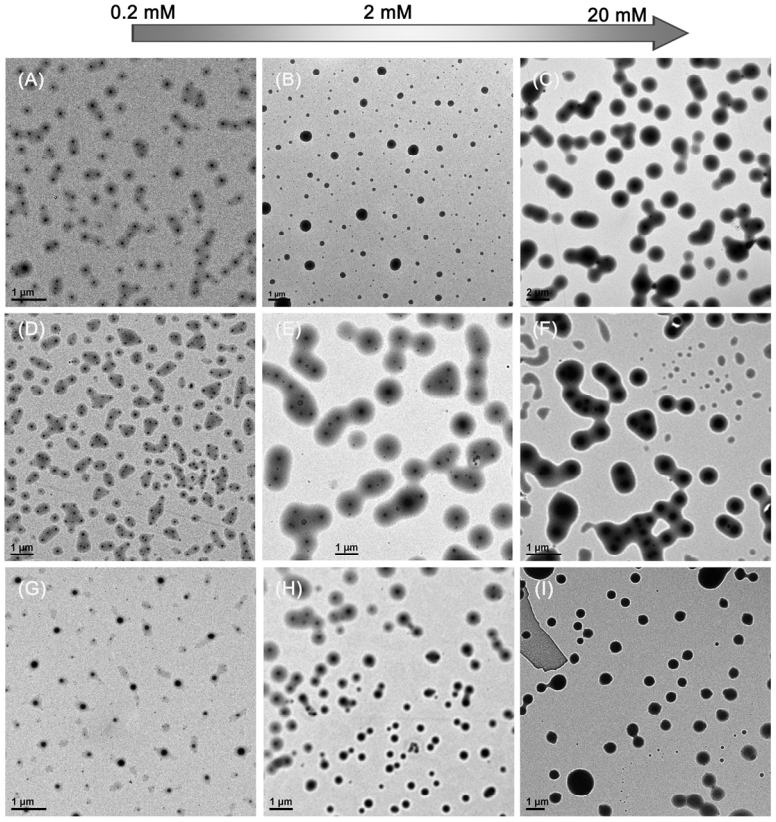

Figure 5. TEM micrographs for drop coating acetone solutions of host-guest (A) ~ (C) G1, (D) ~ (F) G2 and (G) ~ (I) G3 at different concentration.

Moreover, in a different control experiment, the concentration-dependent changes of the self-assembly morphorlogy and size could be observed by TEM analysis. Figure 5 shows the TEM images of particulate G1 ~ G3 at different concentrations. The TEM samples were prepared by simply drop-coating the solution on carbon-coated copper grids, which is the same as method I in preparation of SNPs for fluorescence microscopy testing. Notably, the morphology and size are absolutely different from those of the samples prepared for fluorescence microscopy due to the different substrate (glass slide and copper grid, respectively). The resulting TEM images were included to further demonstrate the biviologen derivatives as structure-directing agents in the self-assembly process is required for SNPs formation and growth.

However, this finding is in contrast to the synthesis of supramolecular nanoparticles by method II. By using method II, we hope the biviologen derivatives can be encapsulated in nanocomplex with controllable morphology and highly stable dispersibility in aqueous solution. This control over the size and shape of self-assembled nanomaterials is of great importance in their biological and clinical applications because the circulation time in vivo and interactions of the nanomaterials with various cells are highly dependent on their size, shape, and surface properties. As can be seen in figure B1~3, the three kinds of viologen derivatives direct toward host **1** in all self-assembly to form micelles in aqueous organic solvent at equivalent concentrations. We can see that the morphology and size of the particles clearly changed when different-length biviologen derivatives and preparation methods were used. Notably, uniformly sized micelles with regular shapes were only produced by host **1** and guest **4** (Group 3), which exhibited high aqueous solubility and stability as compared with corresponding **2** and **3** after emulsion shown in figure S2, and this character has been applied in drug delivery in our present work. The hydrodynamic size of micelles was monitored by dynamic light scattering (table S1), which showed the size from 100 ~ 400 nm at different concentrations. To confirm the fluorescence microscopy results, SEM was used to further monitor the formation of spherical morphologies in aqueous organic solvent systems. As we can see, spherical SNPs were packed on the silica slide (figure S5).

In the light of these encouraging results, a series of self-assemblies were prepared similarly in different concentrations, in order to determine the effects of size of structure-directing agents on the solubility and morphology of these self-assemlies. On the contrary, by using method II, no successful particle formation was observed at total molar concentrations of 0.2 mM and 20 mM of complex in aqueous solution. Instead, small particles and non-uniform aggregates were produced in figure S6.

We found the optimal size had been achieved particularly with a Guest : Host molar ratio of 4 : 1 and a total molar concentration about 2 mM. Because of the use of biviologen derivatives as structure-directing agents in the self-assembly process, this clearly indicates that tetra-calix[4]arene-substituted porphyrin **1**

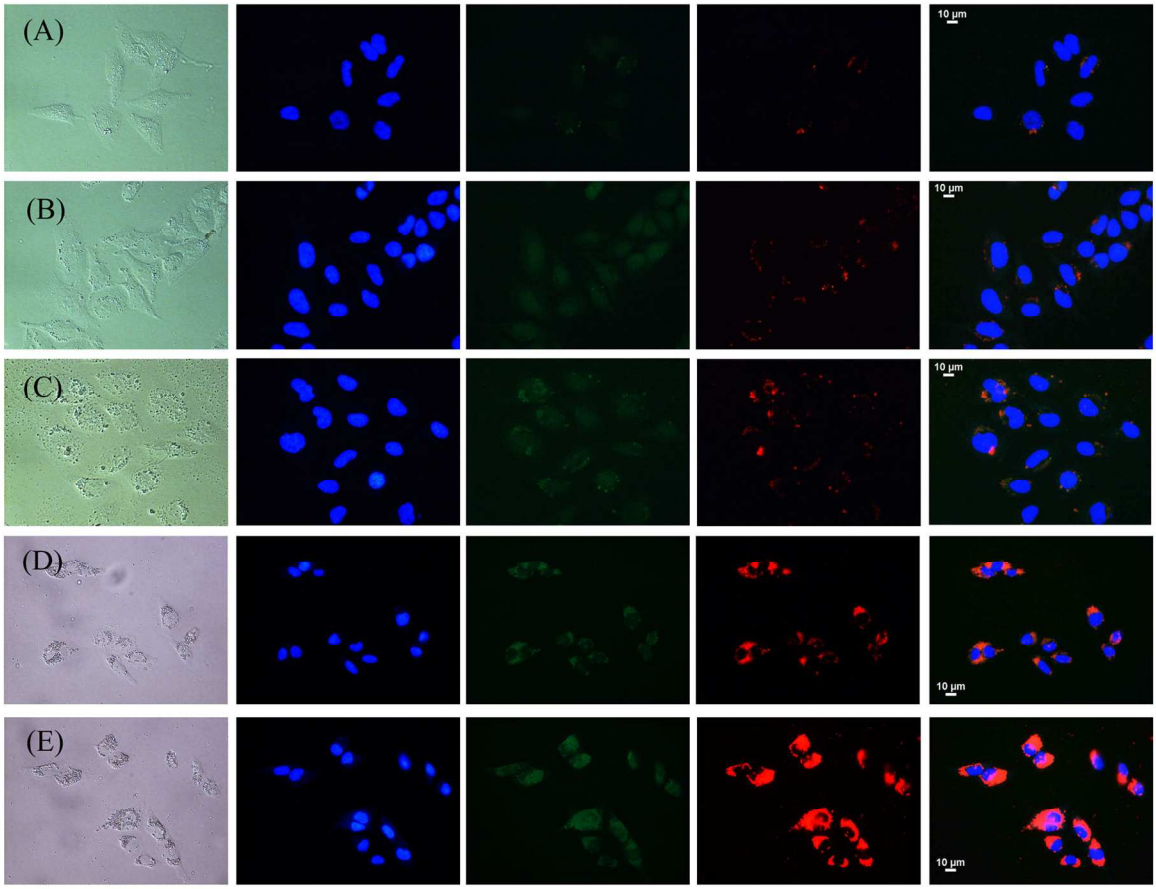

Figure 6. Confocal microscopic images of Hela Cells incubated with SNPs at different concentrations. (A) 0.05 mg/mL; (B) 0.1 mg/mL; (C) 0.4 mg/mL; (D) 1.6 mg/mL; (E) 3.2 mg/mL; Left to right: bright field, Blue channel (405/450 ± 10 nm), FITC (488/525 ± 10 nm), PI channel (488/585 ± 10 nm), merged from Blue, FITC and PI channels. The scale bar is 10 μm.

has successfully formed supramolecular nanoparticles. Further evidence can be seen from control experiments in figure S7 which show that no particle formation was detected by individual component of host and guest on the glass slide. The presence of both host and guest building blocks in the self-assembly process was believed to be crucial factors to form the highly ordered and spherical supramolecular nanoparticles.

Curative effects of supramolecular nanoparticles in solution and in vitro

We next proceeded to investigate the effect of photodynamic therapy approach in vitro by using SNPs as photodynamic therapeutic agent. Before conducting the photodynamic theraphy of SNPs in vitro, we evaluate their performance in solution. Since SNPs originated from G3 through method II are highly stable, they are particularly suitable for this type of studies. To verify the hypothesis, the formation of supramolecular nanoparticles mediated by the host–guest interactions between **1**–**4** with biological activity was initially investigated by using 9,10-anthracenediyl-bis(methylene)dimalonic acid (ABDA) as probe molecule for singlet oxygen generation under light irradiation. Figure S8 shows spectral evolutions of the SNPs in aqueous solution upon irradiation with red light at 633 nm, in which the absorbance of characteristic peaks of ABDA centered at 378 nm gradually decreased with increasing illumination time, indicating that ABDA was oxidized to yield an endoperoxide by singlet oxygen. The capability of free 5,10,15,20-tetrakis(4-hydroxyphenyl)porphyrin **7** to generate singlet oxygen was also recorded under the same condition for direct comparison (Figure S7). Interestingly, the rate of these spectral changes depends on the photo-oxidation of ABDA. Based on the kinetics of the spectral evolution with the decrease of the absorption band at 380 nm, apparent rate constants were derived by fitting the time dependence of the maximum absorbance with an exponential decay (K^a, 1^{st}-order) upon light irradiation (633 nm). Under the same molar concentration of porphyrin fragment in SNPs and free 5,10,15,20-tetrakis(4-hydroxyphenyl)porphyrin **7** in aqueous solution, the resulting decay constants show higher photo-oxidation efficiency of SNPs (4.2×10^{-3} min^{-1}) than that of **7** (2.8×10^{-3} min^{-1}). The increased photo-oxidation efficiency of porphyrin fragment in SNPs may be attributed to the discrete porphyrin fragment in supramolecular network. This result demonstrates that the SNPs are stable and suitable for utilization as photodynamic therapeutic agents.

These encouraging results in solution prompted us to evaluate the feasibility of SNPs as photodynamic therapeutic agents in vitro. First, it is desirable to evaluate the cytotoxicity of the nanomaterial, and their permeability and therapeutic efficiency in vitro. SNPs were first assessed through MTT assay. Different concentrations of SNPs in Dulbecco's Modified Eagle Medium (DMEM) were prepared via serial dilution, and showed high stability (almost constant morphology and dispersibility) up to six months. 7 concentrations ranging from 0.05 mg/mL to 3.2 mg/mL were used for Cell viability assay. The cellular uptake of obtained SNPs was studied by seeding Hela cells at a density of 1×10^5 cells/well on a sterile glass cover slip. Encouragingly, the MTT assay indicates cell viability was not hindered by SNPs up to a concentration of 3.2 mg/mL, thereby revealing good biocompatibility and remarkably low cytotoxicity of SNPs (Figure 7). In addition, we also investigated the behavior of SNPs in living Hela cells. The cells were treated with SNPs at prescribed concentration determined from MTT test. After incubation for 24 hours, cover slips were washed twice with PBS and the cells were fixed using 4% paraformaldehyde (PFA) for 20 min. PFA was subsequently removed and cells were washed twice with PBS before they were examined by confocal microscope. Figure 6 shows the internalization of SNPs into Hela cells, which were incubated with SNPs at different concentration for 24 h. Column A: bright field showing the cell morphology and arrangement. Column B: blue channels showing the DAPI stained nuclei. Column C: FITC channels showing the green fluorescence from SNPs distributed in cytoplasm. Column D: PI channels showing the red fluorescence from SNPs distributed in cytoplasm. Column E: Merged channels of blue, FITC and PI channels. Row 1 ~ 5 with increasing the SNPs, the more fluorescence from SNPs was observersed. These observations indicate that excellent penetration of the SNPs into Hela cells,

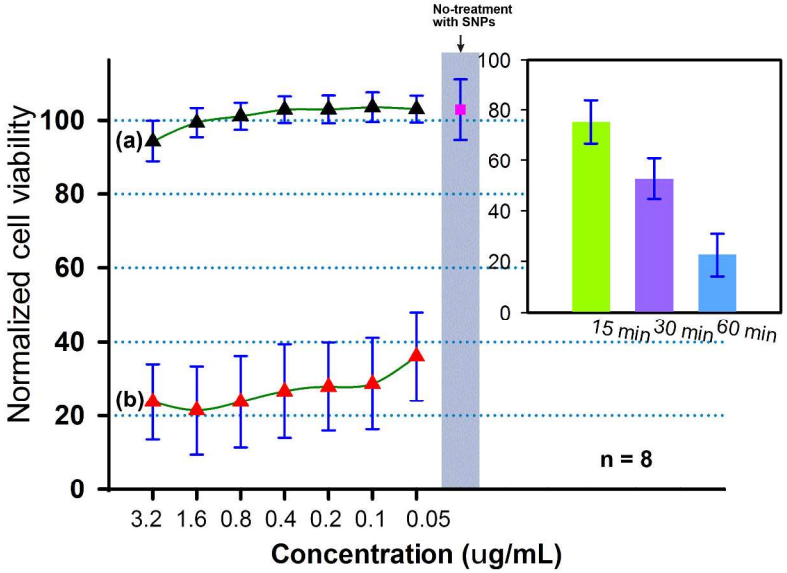

Figure 7. Relative cell viability of HeLa cells after treatment with SNPs at different concentrations (a) no and (b) with light irradiation. Insert: The cell viability at different irradiation time.

and the internalization was concentration-dependent.

If the SNPs were indeed up-taken by Hela cells, the SNPs would generate singlet oxygen under light irradiation and show cytotoxicity to Hela cells. Figure 7 shows the cellular viability measured as a function of concentration using the MTT test after light irradiation for 1 hour. As expected, the results prove this assumption by showing the decrease of cell viability to 20%. Notably, insert of Figure 7 illustrates that the cell viability was decreasing with increasing the irradiation time. In summary, we have demonstrated that SNPs could be successfully endocytosed and show good photosensitization efficiency inside the Hela cells. Therefore, the incovalent immobilization of haematoporphyrin fraction into the supramolecular nanoparticles may lead to an improved system with respect to their permeability and therapeutic efficiency in vitro.

Conclusions

In this study, we have systematically introduced calix[4]arene-decorating tetrameric porphyrin derivative in the presence of three different lengths of biviologen derivatives into the backbone of supramolecular network with controllable morphology. The interfacial method allows us to readily control the domain size and the morphology of SNPs by tuning the guest components. Unambiguous demonstration of the production of the molecularly-engineered nanomaterials could provide a synergistic effect which enables not only the suppression of self-aggregation of photosensitizers but also improvement of photosensitizing efficiency. The in vitro experiments have shown more efficient photodynamic therapy of SNPs as compared with that of pure porphyrin derivative. This observation has also been corroborated by kinetic studies of the photo-oxidation efficiency of ABDA in aqueous solution. Finally, the low cytotoxicity and high photodynamic therapeutic effect of porphyrin-hybrided SNPs in treatment of cancer cells opens a possible pathway for future photodynamic therapeutic applications.

Notes and references

[a] *Institute of Materials Research and Engineering (IMRE), Agency for Science, Technology and Research (A*STAR), 3 Research Link, 11760, Republic of Singapore. Fax: 65 6872 7528; Tel: 65 6872 7543; E-mail: jw-xu@imre.a-star.edu.sg*

[b] *Department of Chemistry, National University of Singapore, 3 Science Drive 3, Singapore 117543, Republic of Singapore*

† Electronic Supplementary Information (ESI) available: [details of any supplementary information available should be included here]. See DOI:

‡ Footnotes should appear here. These might include comments relevant to but not central to the matter under discussion, limited experimental and spectral data, and crystallographic data.

1. D. E. J. G. J. Dolmans, D. Fukumura and R. K. Jain, *Nature reviews. Cancer*, 2003, **3**, 380.
2. a) J. Chen, L. Keltner, J. Christophersen, F. Zheng, M. Krouse, A. Singhal and S.S. Wang, *Cancer Journal*, 2002, **8**, 154; b) S. Yano, S. Hirohara, M. Obata, Y. Hagiya, S. Ogura, A. Ikeda, H. Kataoka, M. Tanaka and T. Joh, *Journal of Photochemistry and Photobiology C: Photochemistry Reviews*, 2011, **12**, 46.
3. L. B. Josefsen and R. W. Boyle, *Metal-based drugs*, 2008, **2008**, 276109.
4. A. P. Thomas, P. S. Saneesh Babu, S. Asha Nair, S. Ramakrishnan, D. Ramaiah, T. K. Chandrashekar, A. Srinivasan and M. Radhakrishna Pillai, *J. Med. Chem.*, 2012, **55**, 5110.
5. D. Bartusik, D. Aebisher, G. Ghosh, M. Minnis and A. Greer, *J. Org. Chem.*, 2012, **77**, 4557.
6. J. T. Lau, P. C. Lo, W. P. Fong and D. K. Ng, *J. Med. Chem.*, 2012, **55**, 5446.
7. T. Zhao, H. Wu, S. Q. Yao, Q. H. Xu and G. Q. Xu, *Langmuir*, 2010, **26**, 14937.
8. M. Lee, S. J. Lee and L. H. Jiang, *J. Am. Chem. Soc.*, 2004, **126**, 12724.
9. X. Shen, F. He, J. Wu, G. Q. Xu, S. Q. Yao and Q. H. Xu, *Langmuir*, 2011, **27**, 1739.
10. P. Han, S. C. Li, W. Cao, Y. Li, Z. Sun, Z. Wang and H. Xu, *J. Mater. Chem. B*, 2013, **1**, 740.
11. J. Voskuhl, U. Kauscher, M. Gruener, H. Frisch, B. Wibbeling, C. A. Strassert and B. J. Ravoo, *Soft Matter*, 2013, **9**, 2453.
12. S. Houmadi, D. Coquiere, L. Legrand, M. C. Faure, M. Goldmann, O. Reinaud and S. Remita, *Langmuir*, 2007, **23**, 4849.
13. Q. Liang, B. Guan and M. Jiang, *J. Mater. Chem.*, 2010, **20**, 8236.
14. S. B. Nimse and T. Kim, *Chem. Soc. Rev*., 2013, **42**, 366.
15. M. R. Hamblin and T. Hasana, *Photochem. Photobiol. Sci.*, 2004, **3**, 436.
16. H. Yan, J. Luo, H. M. Xie, D. X. Xie, Q. Su, J. Yin, B. N. Wanjala, H. Diao, D. L. An and C. J. Zhong, *Phys. Chem. Chem. Phys.*, 2011, **13**, 5824.
17. L. Pescatori, A. Arduini, A. Pochini, A. Secchi, C.Massera and F. Ugozzoli, *Org. Biomol. Chem*., 2009, **7**, 3698.
18. D. S. Guo and Y. Liu, *Chem. Soc. Rev.*, 2012, **41**, 5907.
19. M. Strobel, K. Kita-Tokarczyk, A. Taubert, C. Vebert, P. A. Heiney, M. Chami and W. Meier, *Adv. Funct. Mater.*, 2006, **16**, 252.
20. H. Zhang, K. T. Nguyen, X. Ma, H. Yan, J. Guo, L. Zhu and Y. Zhao, *Org. Biomol. Chem.*, 2013, **11**, 2070.
21. D. S. Guo, K. Wang, Y. X. Wang and Y. Liu, *J. Am. Chem. Soc.*, 2012, **134**, 10244.
22. D. S. Guo, K. Chen, H. Q. Zhang and Y. Liu, *Chem. Asian. J.*, 2009, **4**, 436.
23. M. Fathalla, A. Neuberger, S. C. Li, R. Schmehl, U. Diebold and J. Jayawickramarajah, *J. Am. Chem. Soc.*, 2010, **132**, 9966.
24. G. T. Hwang, B H Kim, *Tetrahedron,* 2002, **58**, 9019.
25. K. Iwamoto, K. Araki and S. Shinkai, *J. Org. Chem.*, 1991, **56**, 4955.